PhotoniX

RESEARCH Open Access

350-2500 nm supercontinuum white laser enabled by synergic high-harmonic generation and self-phase modulation

Lihong Hong[1†], Chenyang Hu[2†], Yuanyuan Liu[1], Huijun He[3], Liqiang Liu[1], Zhiyi Wei[3] and Zhi-Yuan Li[1,4*]

[†]Lihong Hong and Chenyang Hu contributed equally to this work.

*Correspondence: phzyli@scut.edu.cn

[1] School of Physics and Optoelectronics, South China University of Technology, Guangzhou 510641, China
[2] Guangdong Jingqi Laser Technology Corporation Limited, Songshanhu, Dongguan 523808, China
[3] Beijing National Laboratory for Condensed Matter Physics, Institute of Physics, Chinese Academy of Sciences, Beijing 100190, China
[4] State Key Laboratory of Luminescent Materials and Devices, South China University of Technology, Guangzhou 510640, China

Abstract

Supercontinuum white laser with large bandwidth and high pulse energy would offer incredible versatility and opportunities for basic science and high technology applications. Here, we report the generation of high-efficiency 2.8-octave-spanning ultraviolet-visible-infrared (UV-Vis-IR) (with 350-2500 nm 25 dB bandwidth) supercontinuum white laser from a single chirped periodically poled lithium niobate (CPPLN) nonlinear crystal via synergic high-harmonic generation (HHG) and self-phase modulation (SPM). The CPPLN exhibits multiple controllable reciprocal-lattice bands to simultaneously support the quasi-phase matching (QPM) for simultaneous broadband 2nd-10th HHG via cascaded three-wave mixing against a broadband fundamental pump laser. Due to the efficient second-order nonlinearity (2nd-NL) up-conversion and significant 3rd-NL SPM effect both in the pump and HHG laser pulses, 350-2500 nm supercontinuum white laser is eventually obtained with 17 μJ per pulse under pump of 45 μJ per pulse mid-infrared femtosecond laser corresponding to an average high conversion efficiency of 37%. Our work opens up a route towards creating UV-Vis-IR all-spectrum white lasers through engineering the synergic action of HHG and SPM effects in nonlinear crystals for applications in ultrafast spectroscopy, single-shot remote sensing, biological imaging, and so on.

Keywords: Supercontinuum white laser, Quasi-phase matching, High-harmonic generation, Self-phase modulation

Introduction

Supercontinuum white lasers, or supercontinuum generation (SCG) lasers, with broad spectral bandwidth (especially from the ultraviolet across the visible and into the infrared), high spectral flatness, large pulse energy, high peak power, and high temporal and spectral coherence have attracted extensive interest due to a wide range of important applications, such as spectroscopy and microscopy [1, 2], precision frequency metrology [3], pulse compression [4], and optical coherence tomography (OCT) [5, 6]. They are mainly accomplished by harnessing various nonlinear optical effects ignited and driven by high-peak-power pulse lasers. To date, a large number of schemes have been explored and attempted to generate high-quality white lasers with desirable parameters. The most

widely utilized method relies on various third-order nonlinearities (3rd-NL) (self-phase modulation (SPM), four-wave mixing, stimulated Raman scattering, etc) occurring within microstructured photonic crystal fibers [7, 8] or homogeneous plates [9, 10], or noble gas-filled hollow-core fibers [11, 12]. Hence the spectral performance is inexorably tied to the modal area or the dispersion properties of transport waves, which naturally suffers from some limitations, such as unsatisfactory spectral flatness and low pulse energy. For instance, although the SCG has extended down to 200 nm and up to 2500 nm in a solid-core silica-air photonic crystal fiber [8], the spectral broadening is rather localized around the pump wavelength, the spectrum exhibits multiple peaks, and the pulse is at a low energy level. These undesirable weaknesses ultimately degrade the capabilities of spectral scaling up and flatness enhancement towards high-profile SCG lasers. For these reasons, the single 3rd-NL spectral broadening scheme dominantly adopted in the nonlinear optics community has not yet been capable of covering the so-called high-flatness ultraviolet-visible-infrared (UV-Vis-IR) supercontinuum range.

Another well-known scheme to generate broadband laser sources is the second-order nonlinear optical (2nd-NL) effect, including second-harmonic generation (SHG), sum-frequency generation (SFG), differential-frequency generation, parametric oscillation, and amplification processes. As a significant success that is made in the framework of the popular and successful quasi-phase-matching (QPM) theory, chirped periodically poled lithium niobate (CPPLN) nonlinear crystals possessing multiple broadband QPM bands have been extensively investigated to accomplish high-performance laser frequency conversion and expansion via a series of three-wave mixing processes (SHG and SFG) [13–20]. Particularly, it has been shown that the CPPLN schemes can support broadband SHG, simultaneous broadband SHG and third-harmonic generation (THG) [17], and even high harmonic generation (HHG), finally leading to the fascinating ultrabroadband visible white laser [18]. Furthermore, this broadband QPM scheme also allows for collective action of 2nd-NL and 3rd-NL effects to create a tunable visible to near infrared (Vis-NIR) white laser in terms of spectral profile and overall chroma via cascaded broadband SHG and THG [19], and even to build up an intense two-octave spanning UV-Vis-NIR supercontinuum laser via high-efficiency SHG with a fascinating one-octave bandwidth [20]. It is believed that the utilization of synergic action of 2nd-NL SHG (or cascaded SHG and THG interactions combined) and 3rd-NL SPM effect has a significantly enhanced influence on spectral expansion compared with only single 2nd-NL scheme or single 3rd-NL scheme. However, it is also believed that the capability of such a synergic action is still far from bringing into reality the dream of accomplishing supercontinuum laser with extremely broad bandwidth in UV-Vis-IR as well as large pulse power and high peak power.

In this letter, we describe a single CPPLN nonlinear crystal that supports simultaneous 2nd-10th HHG to produce a more than 2.8-octave-spanning supercontinuum white laser by the marriage of 2nd-NL HHG and 3rd-NL SPM effects. We systematically study the QPM process of 2nd-10th HHG in the CPPLN sample that exhibits multiple-order broadband reciprocal lattice vector (RLV) bands and examine their role in driving three-wave mixing up-conversion for a broad bandwidth pump laser. With the interplay of efficient cascaded HHG effects and the remarkable SPM effect induced by a high-peak-power mid-IR pump pulse laser as well as those induced by all the HHG laser pulses,

the CPPLN sample is capable to output a flat supercontinuum laser spectrum across UV-Vis-IR bands ranging from 350 nm to 2500 nm, high energy of 17 μJ per pulse under the pump of 45 μJ per pulse mid-infrared (mid-IR) femtosecond laser, and a record high conversion of 37%. The synergic 2nd-NL and 3rd-NL action scheme presented in this paper can be scaled up to generate high-peak power all-spectrum laser for application to developing novel ultrabroadband and high-dynamic-range spectroscopic technologies, which are very much desirable by researchers working in physics, chemistry, materials, biology, and other fields.

Methods

The principle of ultrabroadband 2nd-10th HHG

There are two vital factors for the realization of high-quality ultrabroadband supercontinuum white laser. One is an input pump laser with a bandwidth as large as possible, hence allowing more frequency components to participate in up-conversion nonlinear processes. The other is a nonlinear material with an operation bandwidth as large as possible to support cascaded up-conversion effects of nonlinear interacting waves. In our work, these two necessary conditions are satisfied based on the basic physics principle of ultrabroadband 2nd-10th HHG together with the synergic action of 2nd-NL and 3rd-NL interactions, which is briefly illustrated in Fig. 1a-b. One can see from Fig. 1a that the femtosecond pulse laser (FW) can ignite simultaneous broadband 2nd-10th HHG signals through a series of cascaded SHG and SFG processes driven by the mere action of single 2nd-NL interaction. However, the naturally limited bandwidth of the pump laser and the resulting smaller bandwidth of each up-conversion harmonic would result in a discontinuous output spectrum, especially between SHG and THG. Nevertheless, if various 3rd-NL processes like SPM are naturally driven by sufficiently high-peak-power pump laser, then firstly, the bandwidth of the pump laser is expanded to some extent, thus bringing an additional degree of freedom into the 2nd up-conversion process. Secondly, the HHG signals will also naturally possess broader up-conversion bandwidth. Thirdly, when the conversion efficiency of HHG is high enough, these high-peak-power HHG pulses still have high enough intensity to ignite considerable 3rd-NL effects to further broaden their own spectral bandwidth and thus enable a broader bandwidth for three-wave mixing 2nd-NL interactions. The consequence of these collective 2nd-NL and 3rd-NL spectral expanding channels is to build up a mechanism to significantly broaden the spectral range of each HHG pulse so that all 2nd-10th HHG pulses have their spectral bands connected with each other without gap and build up an ultrabroadband supercontinuum white laser, as schematically illustrated in Fig. 1b. Simply speaking, HHG and SPM effects cooperate with each other in the designed CPPLN crystal to make this synergic action scheme an ideal route for generating multi-octave-wide supercontinuum white laser with extremely broad bandwidth spanning UV-Vis-IR regimes.

CPPLN design

In the first step, we execute the design of a *z*-cut CPPLN with superior QPM bands in accordance with an effective nonlinear coefficient model [21, 22]. Here, the poling period of CPPLN crystals is described by the formula $\Lambda(y) = \Lambda_0/[1 + (D_g\Lambda_0 y/2\pi)]$ (+ y represents the propagation direction of the pump laser), where D_g is the chirp rate,

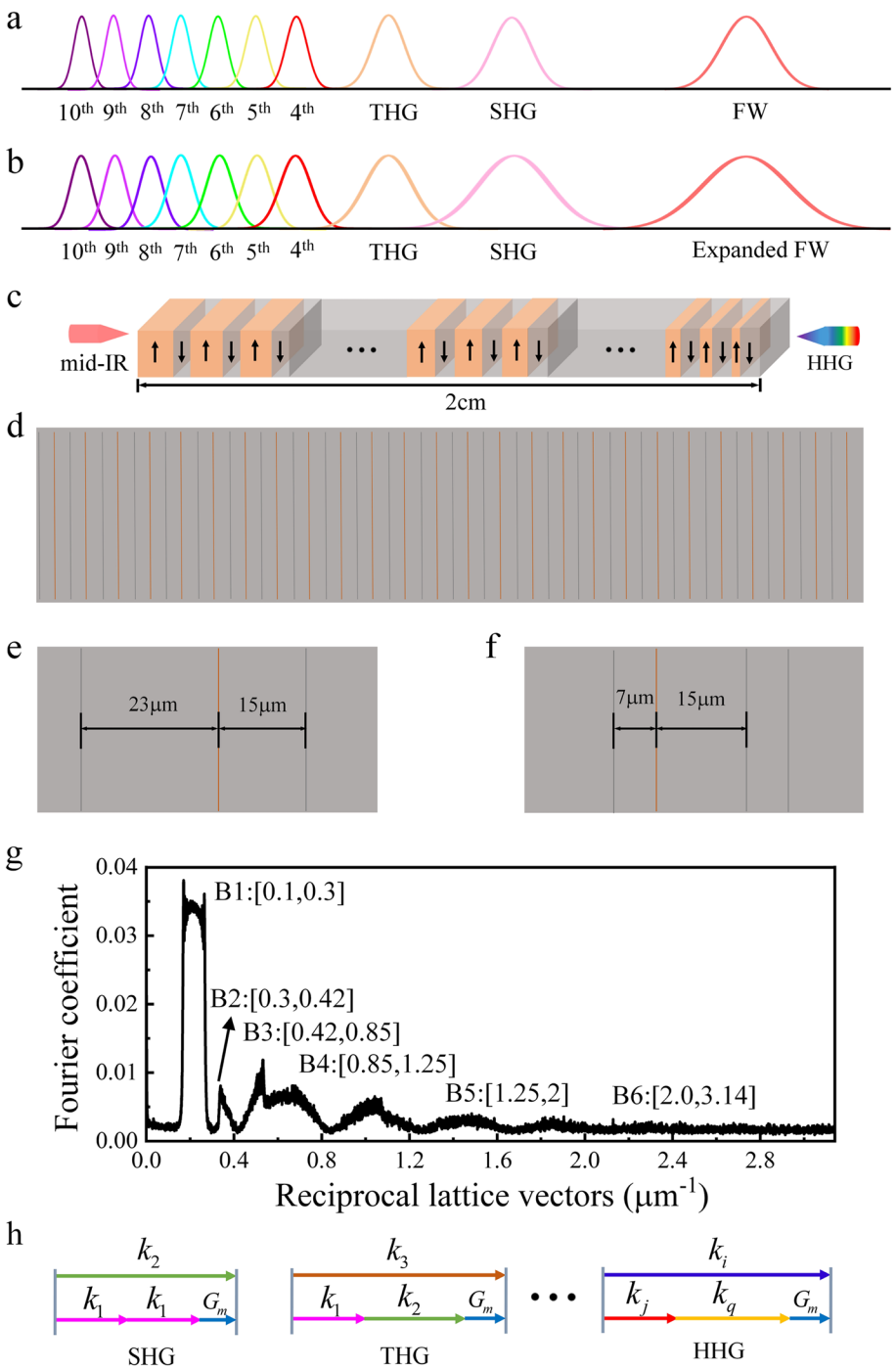

Fig. 1 Principle for supercontinuum white laser generation within CPPLN nonlinear crystal via HHG and SPM effects. **a** Simultaneous broadband 2nd-10th HHG via cascaded 2nd-NL QPM up-conversion upon a mid-IR pump femtosecond laser in CPPLN. **b** Ultrabroadband 2nd-10th HHG supercontinuum white laser upon a high-peak-power mid-IR pump femtosecond laser via synergic action of HHG and SPM effects. **c** Schematic diagram of the structural geometry of the designed CPPLN crystal for HHG. **d** Microscopic image of the etched sample surface of a typical 1D CPPLN structure. **e-f** Enlarged views of two small segments from the left-hand and right-hand portions of the CPPLN sample. **g** Calculated distributions of Fourier coefficient as a function of the RLVs for the designed CPPLN sample. **h** The broadband QPM process of SHG, THG, and HHG

having a significant influence on the conversion efficiency and QPM bandwidth [17]. The optimizing criterion of CPPLN design is based on a compromise among the high-order nonlinear interaction (not only for SHG but also for SFG and THG as well as HHG), the considerable Fourier coefficients, and the available broad QPM band and pump wavelength band. In our work, the central period is deliberately designed to achieve the first-order QPM for SHG at the mid-IR wavelength of 3.6 μm. Figure 1c-f illustrate that the optimized CPPLN structure for realizing HHG is reduced from 38 to 22 μm with the starting period Λ_0 =38 μm, chirp rate D_g =6 μm^{-2}. The poling period consists of a fixed length of negative domain at 15 μm and a varying length of positive domain. That is, the chirp is negative and is obtained by varying the widths of the positive domain. The sample, prepared by standard electric poling technique in a *z*-cut LN crystal doped with 5% MgO [17–22], has a total length of about 20 mm. Typical micrographs of CPPLN samples are explicitly shown in Fig. 1d-f. These continuously varied and asymmetric chirped periods of CPPLN confirm both the odd and even order QPM mechanisms to compensate for the phase mismatching of the multiple broadband upconversion processes. Obviously, the case of an extraordinary light pump is the most beneficial configuration to ignite efficient upconversion processes in such a z-cut CPPLN single crystal, where the largest nonlinear susceptibility component d_{33} of LN material (about 27 pm/V) is adopted. As shown in Fig. 1g, six continuous RLV bands with balanced bandwidth and considerable Fourier coefficients f_G (related to the effective second-order nonlinear coefficients via $\chi_G^{(2)} = d_{33} f_G$) can be achieved from our designed CPPLN sample. These RLV bands are located at [0.1, 0.3] for band B1, [0.3, 0.42] for band B2, [0.42, 0.85] for band B3, [0.85, 1.25] for band B4, [1.25, 2.0] for band B5, and [2.0, 3.14] for band B6, all in units of μm^{-1}. Band B1 exhibits the largest effective nonlinear coefficients, reaching a modest large value around 0.035 d_{33}, while the other bands show smaller effective nonlinear coefficient, but still at a level 0.005-0.01 d_{33}. Note that these nonlinear coefficients are far smaller than that of LN crystal, but under the pump of high-peak power femtosecond pulse laser, the 2nd-NL interactions are still significant. The effective QPM processes come from the moment when specific wave-vector mismatch Δk (as defined in Table 1) is successfully compensated by the appropriate RLV bands G_m ($G_m = m2\pi/\Lambda(y)$, m representing the QPM order) of the CPPLN sample. They work together and allow

Table 1 Contribution of QPM band and specific QPM three-wave mixing processes to various-order HHG. k_i is the wave number of the *i*th HHG wave within a nonlinear crystal

HHG	Phase mismatching in three-wave mixing processes	QPM band
2nd HG	$\Delta k_1 = k_2 - 2k_1$	B1
3rd HG	$\Delta k_2 = k_3 - k_2 - k_1$	B1
4th HG	$\Delta k_3 = k_4 - k_3 - k_1$, $\Delta k_4 = k_4 - 2k_2$	B1, B2
5th HG	$\Delta k_5 = k_5 - k_4 - k_1$, $\Delta k_6 = k_5 - k_3 - k_2$	B2, B3
6th HG	$\Delta k_7 = k_6 - k_5 - k_1$, $\Delta k_8 = k_6 - k_4 - k_2$, $\Delta k_9 = k_6 - 2k_3$	B2, B3, B4
7th HG	$\Delta k_{10} = k_7 - k_6 - k_1$, $\Delta k_{11} = k_7 - k_5 - k_2$, $\Delta k_{12} = k_7 - k_4 - k_3$	B3, B4, B5
8th HG	$\Delta k_{13} = k_8 - k_7 - k_1$, $\Delta k_{14} = k_8 - k_6 - k_2$, $\Delta k_{15} = k_8 - k_5 - k_3$, $\Delta k_{16} = k_8 - 2k_4$	B3, B4, B5
9th HG	$\Delta k_{17} = k_9 - k_8 - k_1$, $\Delta k_{18} = k_9 - k_7 - k_2$, $\Delta k_{19} = k_9 - k_6 - k_3$, $\Delta k_{20} = k_9 - k_5 - k_4$	B4, B5, B6
10^{th}HG	$\Delta k_{21} = k_{10} - k_9 - k_1$, $\Delta k_{22} = k_{10} - k_8 - k_2$, $\Delta k_{23} = k_{10} - k_7 - k_3$, $\Delta k_{24} = k_{10} - k_6 - k_4$, $\Delta k_{25} = k_{10} - 2k_5$	B4, B5, B6

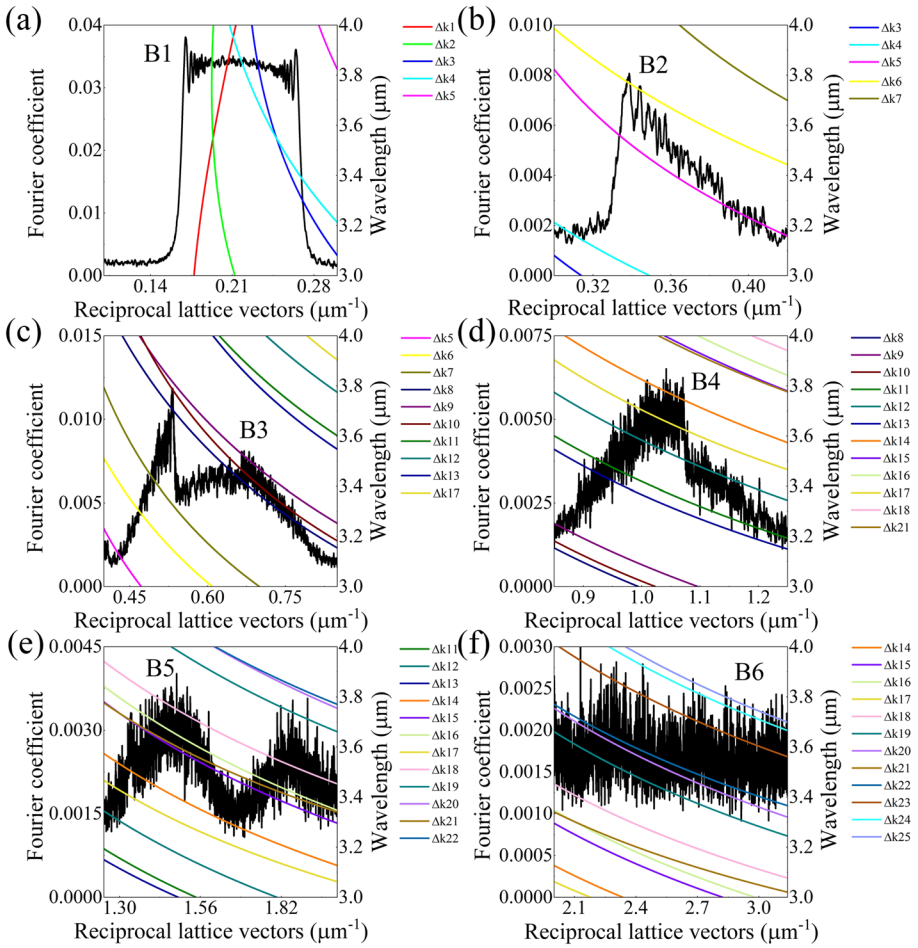

Fig. 2 QPM schemes in CPPLN for 2nd-10th HHG based on broadband three-wave mixing processes. **a-f** Collective plots of the Fourier coefficient curves in band B1-B6 offered by the CPPLN structure and the phase mismatch curves of various three-wave mixing processes in a homogeneous LN crystal that are adopted to accomplish 2nd-10th HHG. The efficient QPM three-wave mixing process arises from the overlap between the two curves within the given mid-IR pump laser band

for efficient HHG via a series of cascaded SHG and SFG interactions, as concretely sketched in Fig. 1h.

QPM scheme of 2nd-10th HHG

In order to clearly evaluate the up-conversion performance of the designed CPPLN crystal in the QPM scheme, we calculate the distributions of the effective nonlinear coefficient as functions of the RLVs for the sample and the phase-mismatch curves for 2nd-10th HHG three-wave mixing processes, and plot them collectively in Fig. 2a-f. As clearly plotted in Fig. 2a, the wave-vector mismatching Δk_1 and Δk_2, corresponding to SHG and THG, are completely covered by the RLV band of B1 with the largest Fourier coefficient, thus the B1 band provides a possibility to realize efficient SHG and THG process over the wide pump range from 3000 to 4000 nm. Meanwhile, SHG and THG act as the initial signals to generate higher-order harmonics via cascaded SHG and SFG processes against lower-order harmonics. The QPM procedures in the designed CPPLN

sample are displayed in Fig. 2b-f. Looking closely into Fig. 2b, the 4th HHG mainly results from the effective compensation of B1 band to the curves Δk_3 in pump band 3300-4000 nm and Δk_4 in pump band 3390-4000 nm. It is worth noting that one part of QPM processes for the 4th HHG in the short-wavelength part lies in the band gap between band B1 and band B2 with a lower Fourier coefficient, thus the conversion efficiency of the 4th HHG will be vastly reduced. According to Fig. 2c-f, the generation of 5th HHG comes from the fulfillment of QPM by bands B2 and B3 dominantly through the Δk_6 process in the overall pump region. It is expected that the 5th HHG will show a considerable conversion efficiency arising from a cascade action of high-intensity SHG and THG within Δk_6 process.

QPM for the 6th HHG via the Δk_7, Δk_8, and Δk_9 processes can be automatically achieved by the RLV bands of B2, B3, and B4 in the whole pump band. Moreover, the second highest Fourier coefficient in band B3 among all six RLV bands (see Fig. 1g) will create a high level of conversion efficiency for the 6th HHG. Bands B3, B4, and B5 contribute towards fulfillment of the QPM interactions for the 7th HHG via the required wave-vector processes Δk_{10}, Δk_{11}, and Δk_{12}. Moreover, all three processes come from the cascaded processes of relatively high-intensity harmonics accompanied by effective QPM bands of large bandwidth, which ensures the high efficiency of 7th HHG. The phase mismatches Δk_{13}, Δk_{14}, Δk_{15}, and Δk_{16} for the 8th HHG are effectively compensated by bands B2, B3, and B5. In this case, there is a compromise between the relatively low nonlinear coefficient and the available broad QPM band. Thus, the efficiency of 8th HHG might not be high, but it is still observable. The same compromise law also holds for the 9th and 10th HHG cases. Here, the 9th HHG is enabled by four processes $\Delta k_{17} - \Delta k_{20}$ via bands B4, B5, and B6, while the 10th HHG is supported by five processes $\Delta k_{21} - \Delta k_{25}$ via the same RLV bands. It is good to see that such a specially designed CPPLN sample with multiple RLV bands interconnecting each other with almost no gap, will be capable of simultaneously accomplishing broadband multi-order HHG against a broadband and high-peak-power pump femtosecond laser, and therefore lead to the output of an ultrabroadband supercontinuum white laser.

Results and discussion

Experiment of HHG against mid-IR pump laser

The schematic setup for measuring and analyzing the supercontinuum spectrum emitted from the CPPLN sample is presented in Fig. 3a. The pump laser, being at a horizontal polarization state (namely, extraordinary light state), is a mid-IR femtosecond laser based on a home-built optical parametric amplification device [23], with a tunable center-wavelength mid-IR band from 2.86 to 3.6 μm. In our experiment, the central wavelength of the mid-IR femtosecond laser is adjusted to 3.6 μm to match the CPPLN sample design, with a repetition rate of 1 kHz, a pulse duration of 120 fs, corresponding to a pulse full width at half maximum (FWHM) bandwidth of around 357 nm, a setting pulse energy 45 μJ and average power of 45 mW, corresponding to a peak power of 0.38 GW (Fig. 3b). The pump beam is directed at the *xz* surface of the *z*-cut CPPLN crystal with an $f = 200$ mm CaF_2 lens creating a spot size around 0.5 mm. This configuration confirms that the electric field is parallel to the surface normal of the *z*-cut LN planar slab. The corresponding peak intensity of 190 GW/cm^2 is well below the optical damage

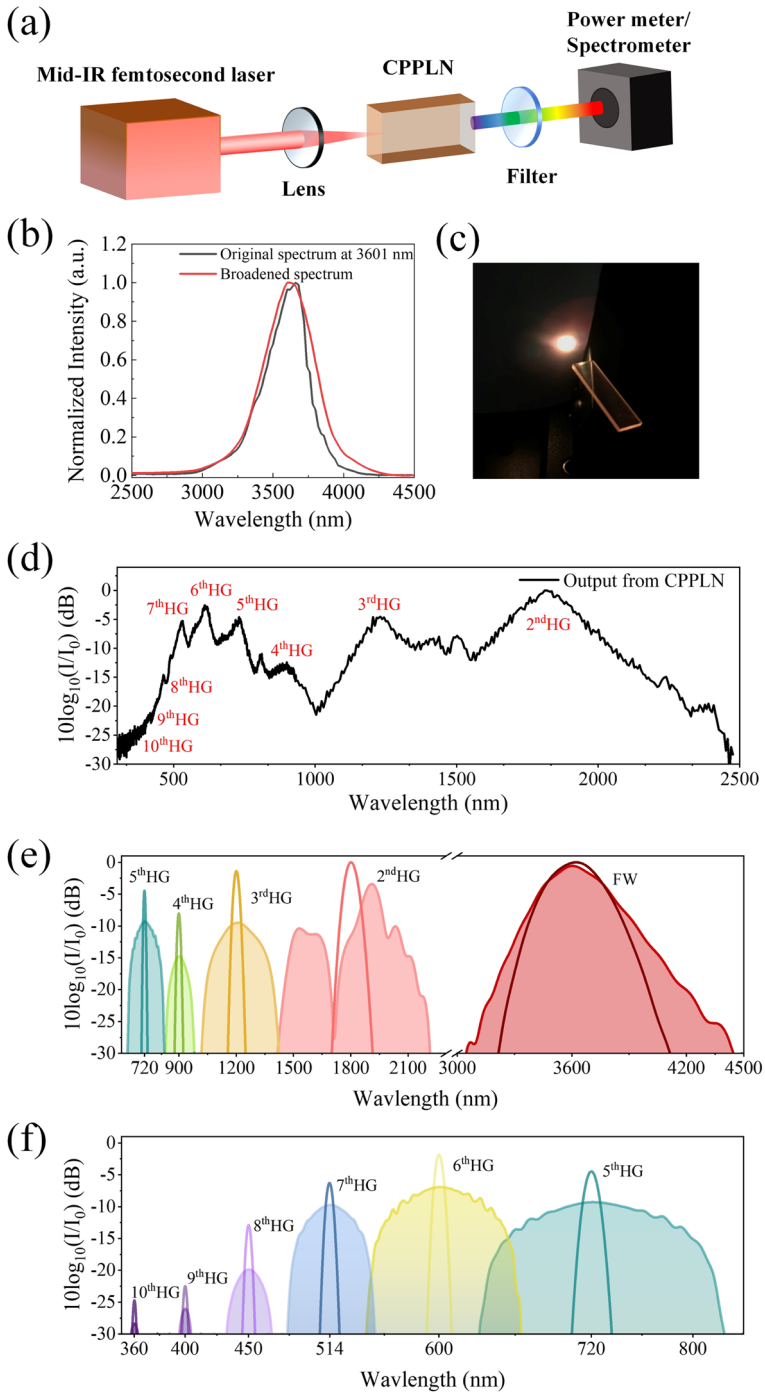

Fig. 3 **a** Schematic diagram of the experimental setup. Here, the mid-IR pump beam, being at a horizontal polarization state (namely, extraordinary light state) is incident upon the *xz* surface of the *z*-cut CPPLN crystal. **b** Spectral broadening for the pump laser pulse with central wavelength 3601 nm passing through a bare LN crystal. **c** Photograph of a dazzling output white-laser spot emitted from the designed CCPLN sample (with a dimension in length, width, and thickness of 20 mm × 6 mm × 2 mm) under the pump of the mid-IR femtosecond laser. **d** Normalized spectrum of the output HHG signals generated by mid-IR femtosecond laser via synergic HHG and SPM effects as estimated by a criterion of − 25 dB. Note that the spectrum has been normalized against the maximum value. **e-f** The numerical simulations of SPM spectral broadening of the mid-IR pump laser and 2nd-10th HHG pulses in the NLSE model. The light-colors filled areas represent the SPM broadened curves corresponding to their original laser signals (marked by darker colors)

threshold of the sample, but sufficient to ignite significant 3rd-NL SPM processes, not to say various 2nd-NL three-wave mixing processes. As clearly displayed in Fig. 3b, the output spectrum after the pump laser passes through a bare LN crystal exhibits a significant SPM broadening effect and the bandwidth is increased from 357 to 423 nm. Similar SPM broadening should occur for the CPPLN sample. This means there are more frequency components of the pump laser to participate in the 2rd-NL up-conversion processes within the CPPLN sample. The observed bright spot emitted from the CPPLN crystal under the illumination of the mid-IR femtosecond laser is displayed in Fig. 3c, preliminarily showing the efficient generation of an ultrabroadband bright laser beam. Clearly, the output SH beam manifests a basically complete circular spot shape and maintains the original profile of the pump light beam. This is a direct reflection of the good spatial coherence of the output white laser beam. In the next step, we use two optical spectrometers to make an accurate spectral analysis over this output white laser light beam: a UV-Vis spectrometer (Ocean Optics HR 4000, 340-1040 nm) and an IR spectrometer (Ocean Optics NIR quest, 900-2500 nm). By means of power calibration, we calibrate the two collected spectra by interpolating the data and stitching them together in a shared region where both spectrometers are reasonably effective. The result of the output spectral profile is illustrated in Fig. 3d.

Figure 3d shows notable spectral continuity and smoothness in a large range around 350-2500 nm encompassed by the whole 2nd-10th HHG processes, which is a good illustration of the spatial coherence of the output spectra in terms of good ultrabroadband uniformity. In addition, the peaks of these up-conversion bands are located at around 1817, 1228, 896, 730, 612, 528, 464, and 365 nm, respectively, corresponding well to the 2nd-10th HHG of the mid-IR pump central wavelength. On the other hand, the initial bandwidth of the pump laser is 357 nm. Then, if considering only the 2nd-NL effects, the bandwidth of SHG and THG would be at the value of 179 and 119 nm, respectively, which would be far away from connecting the SHG and THG bands each other without any gap. Similarly, the spectra of 4th-10th HHG would show narrower pulse bandwidths, and they altogether cannot cover the entire broadband UV-Vis band with no gaps, as observed in experiments. Things change dramatically when all involved 2nd-NL and 3rd-NL effects for 2nd-10th HHG are taken into account simultaneously to address the supercontinuum output, according to the principle presented in Fig. 1b. Compared with HHG using only a direct 2nd-NL up-conversion configuration [18], the marriage of 2nd-NL HHG and 3rd-NL SPM schemes help to reach a UV-Vis-IR supercontinuum output involving spectrum-interconnecting 2nd-10th HHG covering 350-2500 nm (see Fig. 3d), and at the same time, maintain high conversion efficiency for each HHG and overall supercontinuum white laser.

We proceed to analyze the energy conversion efficiency of this ultrabroadband HHG interaction by quantifying the power of each-order HHG beam. After passing through the sample the residual pump laser is blocked by an appropriate bandpass filter. Here, the power of the pump laser is set to 45 mW. The average power of the up-conversion supercontinuum output is calculated to be about 17 mW, corresponding to a high conversion efficiency of 37%. More specifically, the conversion efficiency of 2rd-10th HG is estimated to be 22.09%, 7.22%, 0.82%, 2.31%, 3.05%, 1.09%, 0.18%, 0.11%, and 0.07%, respectively, as summarized in Table 2. The total power of 2nd and 3rd HHG signals

Table 2 Estimated conversion efficiency of the 2nd-10th HHG upon the input pump power of 45 mW

HHG	Average power of the up-conversion supercontinuum (mW)	Up-conversionefficiency
2nd HG	9.94	22.09%
3rd HG	3.25	7.22%
4th HG	0.37	0.82%
5th HG	1.04	2.31%
6th HG	1.37	3.05%
7th HG	0.49	1.09%
8th HG	0.08	0.18%
9th HG	0.05	0.11%
10th HG	0.03	0.07%

in the NIR band is 3 times that of 4th-10th HHG in the UV-Vis band. Additionally, the 6th HHG has a much higher efficiency than any other harmonics in the UV-Vis spectrum. These features all agree quite well with our previous analysis of QPM processes for various-order HHG as displayed in Fig. 2. This is a further proof that we can deeply tailor and optimize the controllable QPM bandwidth within the CPPLN sample through best estimates of energy ratio and conversion efficiency, and create a white laser of larger bandwidth and better spectral profile and flatness. It is worth mentioning that the supercontinnum laser emission from CPPLN shows no degradation both in power and spectral shape, even after runtime for 7-8 hours every day over a period of several weeks. This shows a good feature of a long-term power stability from the supercontinuum output.

In previous works, the quality of SCG sources has been subject to some certain limitations, such as small pulse energy at nanojoule level [7, 8, 27–29], the 20 dB bandwidth difficult to exceed two octaves [11, 12, 30, 32, 33], usage of fiber-integrated tedious optical components, the need of complicated dispersion-engineering [8, 31–34], and so on. Here, one of the reports shows that a coherent 'light bulb' spanning six octaves (from 350 nm to 22,500 nm) can be achieved by the ultralow-noise Er:fibre comb technology, however, the intensity of the edge spectrum is limited to a very low level of only − 60 dB and the 50 nJ regime [32]. The similar case exists in Ref. [33], that is, supercontinuum output with nearly seven octave bands is obtained, but with a spectral range of 340-40,000 nm at a much lower level dB bandwidth and a single pulse energy of only 0.45 μJ. Another report demonstrates a 51.5 W supercontinuum spanning 405 nm to 2660 nm with endlessly single mode output, but also greatly restricted by the complicated master oscillator power amplifier type architecture and unfavorable spectral multi-peak properties [34]. It can be said that the SCG spectrum obtained by pure third-order nonlinear effects of the microstructure fiber has many obnoxious limitations.

In contrast, our current scheme, a particularly simple way of utilizing the HHG and SPM effects of CPPLN nonlinear crystals, has involved a series of advantages for constructing a high-quality supercontinuum white femtosecond laser. First, this technology, taking advantage of the synergic action of HHG and SPM effects, subtly depends on pump laser conditions and versatile QPM capability in terms of spectral intensity, bandwidth, flattness, and chroma. This greatly escapes the limitations of cumbersome dispersion engineering, spectral multiple-peak, and low pump energy levels in regular

microstructured fiber optical systems. Second, this experimental architecture is simple, easy to carry out, stable, and free from complicated optical setups and infrastructures. Under such a distinguished configuration, the obtained ultrabroadband supercontinuum output has demonstrated superior performances, with not only an extremely large bandwidth (spanning 2.8 octaves), but also high-flatness spectral profile (from 350 to 2500 nm with a flatness better than 25 dB, and from 400 nm to 2400 nm with a flatness better than 20 dB), large pulse energy (17 μJ per pulse), and high average and peak power as well as long-term power stability.

Numerical simulations of SPM spectral broadening

It is natural to ask for a more thorough interpretation about the influence of 3rd-NL SPM processes in such a collective scheme. To this task, we introduce the simplified nonlinear Schrödinger equation (NLSE) to include the linear dispersion and SPM effects to simulate the broadening evolution of the HHG pulses during their transmission through the CPPLN sample [24–26]. In this calculation, we set ten initial Gaussian pulses with the same bandwidth of 120 fs, in which the central wavelengths of harmonics are 2-10 times the initial pump central wavelength at 3600 nm, respectively. Then, we set the energy of the HHG pulses as equal to the experimentally recorded values displayed in Table 2. As illustrated in Fig. 3e-f, the pump laser and each HHG output both have an obvious 3rd-NL SPM broadened bandwidth. More specifically, the FW pump beam is observed with an expanded band of 3125-4306 nm corresponding to the original range of 3243-4054 nm, counted at a − 25 dB intensity level. In the same manner, the 2nd-8th HHG encompass a sequence of broadened broadband frequency domains of 1431-2204 nm, 1027-1412 nm, 836-973 nm, 636-820 nm, 545-663 nm, 482-549 nm, and 436-465 nm, much broader that the original values of 1710-1904 nm, 1160-1245 nm, 881-921 nm, 707-735 nm, 592-610 nm, 507-521 nm, and 446-456 nm, respectively. As for the 9th-10th HHG, which are at a lower pulse energy level, there are only slight signal as estimated by − 30 dB with almost no broadening to occur. The spectral evolution calculation results provide a good description of the experimental HHG spectra as to the SPM effects, while the agreement between the measured and calculated spectral profiles is not good enough.

To account for this discrepancy, we note that some part of the harmonics energy is used for the conversion into higher order harmonics, the other part is used for their own SPM broadening, and they show a competitive relationship with each other. Moreover, the magnitude of SPM spectral broadening greatly depends on the pulse power density. At present, we have simply assumed that all the recorded energy of each-order HHG output is used for SPM broadening. In this sense, the simulated 3rd-NL broadening effect is stronger than the actual one. Even under such a stronger SPM broadening, the output spectrum of the 2nd-10th HHG is still not connected with each other. In the − 25 dB level, there still exist 5 to 40 nm spectral gaps among the expanded bands of 2nd-5th HHG. Even in the − 30 dB level, the gaps among 7th-10th HHG are obviously observable. These features are of course far from being in good agreement with the experimental results. This means that the above three-step sequential action model: 3rd-NL spectral broadening of FW pulse, 2nd-NL HHG, and 3rd-NL spectral broadening of HHG pulses, is not a satisfactory physical model for the true nonlinear optical interaction

processes occurring and generating the 350-2500 nm supercontinuum white laser. In fact, this three-step action model has neglected the 2nd-NL interactions between spectrum-broadened HHG pulses. Thus, we believe that the further three-wave mixing processes of the expanded frequency elements in FW and HHG lasers are indispensable to accurately account for the final balanced supercontinuum white laser generation encompassing an extremely wide range of UV-Vis-IR wavelengths. When the 2nd-NL effect is introduced as new ingredient to describe the nonlinear coupling among the 3rd-NL spectrum-expanded pump laser and HHG pulses, a series of harmonics at new wavelengths will be created and mixed through SHG and SFG processes. As a consequence of this three-wave mixing, we expect an expansion of the overall supercontinuum spectral profile and filling-in of the spectral gaps among various HHG, and eventually the formation of supercontinuum white laser with spectral range of 350-2500 nm. Definitely, the nonlinear dynamics of balanced ultrabroadband HHG supercontinuum laser from the CPPLN sample need to be understood by reference to the synergic regime of HHG and SPM effects rather than a separate and cascaded action of single 2nd-NL or 3rd-NL interaction in a way that has been described in Fig. 1a-b. For simpler words, one must take into full account the synergic action of 2nd-NL HHG and 3rd-NL SPM spectral broadening and their strongly interwinding actions in order to better understand the physics, engineer the properties, and explore the applications of the 350-2500 nm supercontinuum white laser.

Conclusion

In summary, we have designed and fabricated a CPPLN nonlinear crystal to realize a 2.8-octave ultrabroadband UV-Vis-IR white laser (with 350-2500 nm 25 dB bandwidth) via a synergic action of 2nd-NL HHG and 3rd-NL SPM interactions, with the output energy of 17 μJ under pump of 45 μJ per pulse and a high conversion efficiency up to 37%. This series of breakthroughs in extending and improving the crucial property and quality of supercontinuum white laser light sources can be attributed to the following factors. First, the 3rd-NL SPM spectral broadening of mid-IR pump laser induced by high peak power mid-IR pump laser induces more spectral components to take part in the ultrabroadband 2nd-NL up-conversion processes within the CPPLN sample. Second, the designed CPPLN sample offers sufficient-broadband and high-efficiency QPM bands to support simultaneous 2nd-10th HHG against the broadband mid-IR spectrum-expanded pump laser. Third, the high-intensity up-conversion HHG pulses have their own SPM effect due to the sufficiently high peak power, triggering a new round of 3rd-NL SPM spectral expansion. Moreover, the expanded HHG output pulses further participate in the broadband 2nd-NL three-wave mixing processes (SHG and SFG) to achieve harmonic signals at new wavelengths. The synergic and interwinding action of all these three collective physical processes make a major contribution to generate ultrabroadband HHG, and finally, create a smoother and flatter supercontinuum white laser encompassing an extremely broad spectrum across 350-2500 nm.

The CPPLN scheme with enabled QPM processes of 2nd-10th HHG by harnessing the synergic action of both HHG and SPM effects provides a significant route for constructing a supercontinuum white femtosecond laser with desirable parameters in terms of pulse energy and intensity, spectral bandwidth, spectrum flatness, and operation

stability. Such a superior UV-Vis-IR supercontinuum white laser can find potential applications in a variety of basic science and high technology areas such as large-screen laser displays, supercontinuum laser sources, optical combs, and optical communication. Additionally, we envision that these experiences of engineered 2nd-NL and 3rd-NL interactions and couplings within nonlinear materials enabling the synergic action of HHG and SPM effects will provide a powerful guidance for accomplishing the dream of ultra-intense all-spectrum white laser covering an extremely broad range from ultraviolet to mid-infrared (300-5500 nm), simultaneously with smooth and flat spectral profile, large pulse energy and peak power densities, and high spatial and temporal coherence. We believe this groundbreaking high-performance white laser will bring promisingly much better techniques and tools for applications of full-spectrum, ultrafast, single-shot spectroscopies in physics, chemistry, biology, material science, and other disciplines.

Acknowledgements
Not applicable.

Authors' contributions
Z. Y. Li supervised the project. Z. Y. Li, L. H. Hong and C. Y. Hu conceived and designed the experiments, L. H. Hong and C. Y. Hu performed the design of CPPLN crystal and carried out the experiments, Y. Y. Liu offered assistance in theoretical calculations. L. H. Hong and Z. Y. Li provided the theoretical and experimental analysis, and wrote the manuscript. All authors participated in the discussion of results and reviewed the manuscript. The author(s) read and approved the final manuscript.

Funding
The authors are grateful for the financial support from the National Natural Science Foundation of China (11974119), Science and Technology Project of Guangdong (2020B010190001), Guangdong Innovative and Entrepreneurial Research Team Program (2016ZT06C594), and National Key R&D Program of China (2018YFA 0306200).

Availability of data and materials
The data that support the findings of this study are available from the authors on reasonable request.

Declarations

Ethics approval and consent to participate
There is no ethics issue for this paper.

Consent for publication
All authors agreed to publish this paper.

Competing interests
The authors declare that they have no competing interests.

Received: 22 November 2022 Revised: 8 February 2023 Accepted: 28 February 2023
Published online: 09 March 2023

References

1. Dudley JM, Taylor JR. Supercontinuum generation in optical fibers. New York: Cambridge University Press; 2010.
2. Diaspro A, Bianchini P, Vicidomini G, Faretta M, Ramoino P, Usai C. Multi-photon excitation microscopy. Biomed Eng Online. 2006;5:1–14.
3. Udem T, Holzwarth R, Hansch TW. Optical frequency metrology. Nature. 2002;416:233–7.
4. Mollenauer LF, Stolen RH, Gordon JP, Tomlinson WJ. Extreme picosecond pulse narrowing by means of soliton effect in single-mode optical fibers. Opt Lett. 1983;8:289–91.
5. Froehly L, Meteau J. Supercontinuum sources in optical coherence tomography: a state of the art and the application to scan-free time domain correlation techniques and depth dependant dispersion compensation. Opt Fiber Technol. 2012;18:411–9.
6. Ji XC, Mojahed D, Okawachi Y, Gaeta AL, Hendon CP, Lipson M. Millimeter-scale chip-based supercontinuum generation for optical coherence tomography. Sci Adv. 2021;7:eabg8869.
7. Russell P. Photonic crystal fibers. Science. 2003;299:358–62.
8. Jiang X, Joly NY, Finger MA, Babic F, Wong GKL, Travers JC, et al. Deep-ultraviolet to mid-infrared supercontinuum generated in solid-core ZBLAN photonic crystal fiber. Nat Photonics. 2015;9:133–9.
9. He P, Liu YY, Zhao K, Teng H, He XK, Huang P, et al. High-efficiency supercontinuum generation in solid thin plates at 0.1 TW level. Opt Lett. 2017;42:474–7.

10. Su YB, Fang SB, Gao YT, Zhao K, Chang GQ, Wei ZY. Efficient generation of UV-enhanced intense supercontinuum in solids: toward sub-cycle transient. Appl Phys Lett. 2021;118:261102.
11. Hassan MT, Luu TT, Moulet A, Raskazovskaya Q, Zhokhov P, Garg M, et al. Optical attosecond pulses and tracking the nonlinear response of bound electrons. Nature. 2016;530:66–70.
12. Mucke OD, Fang SB, Cirmi G, Rossi GM, Chia SH, Ye H, et al. Toward waveform nonlinear optics using multimillijoule sub-cycle waveform synthesizers. IEEE J Sel Top Quantum Electron. 2015;21:8700712.
13. Armstrong JA, Bloembergen N, Ducuing J, Pershan PS. Interactions between light waves in a nonlinear dielectric. Phys Rev. 1962;127:1918–39.
14. Zhu SN, Zhu YY, Qin YQ, Wang HF, Ge CZ, Ming NB. Experimental realization of second harmonic generation in a Fibonacci optical Superlattice of $LiTaO_3$. Phys Rev Lett. 1997;78:2752–5.
15. Chen BQ, Zhang C, Liu RJ, Li ZY. Multi-direction high-efficiency second harmonic generation in ellipse structure nonlinear photonic crystals. Appl Phys Lett. 2014;105:151106.
16. Zhu SN, Zhu YY, Ming NB. Quasi-phase-matched third-harmonic generation in a quasi-periodic optical super-lattice. Science. 1997;278:843–6.
17. Chen BQ, Ren ML, Liu RJ, Zhang C, Sheng Y, Ma BQ, et al. Simultaneous broadband generation of second and third harmonics from chirped nonlinear photonic crystals. Light Sci Appl. 2014;3:e189.
18. Chen BQ, Zhang C, Hu CY, Liu RJ, Li ZY. High-efficiency broadband high-harmonic generation from a single quasi-phase-matching nonlinear crystal. Phys Rev Lett. 2015;115:083902.
19. Chen BQ, Hong LH, Hu CY, Li ZY. White laser realized via synergic second- and third-order nonlinearities. Research. 2021;2021:1–13.
20. Li MZ, Hong LH, Li ZY. Intense two-octave ultraviolet-visible-infrared supercontinuum laser via high-efficiency one-octave second-harmonic generation. Research. 2022;2022:1–9.
21. Ren ML, Li ZY. An effective susceptibility model for exact solution of second harmonic generation in general quasi–phase-matched structures. EPL. 2011;94:44003.
22. Hu CY, Li ZY. An effective nonlinear susceptibility model for general three-wave mixing in quasi-phase-matching structure. J Appl Phys. 2017;121:123110.
23. He HJ, Wang ZH, Hu CY, Jiang JW, Qin S, He P, et al. 520-μJ mid-infrared femtosecond laser at 2.8 μm by 1-kHz KTA optical parametric amplifier. Appl Phys B Lasers Opt. 2018;124:1–5.
24. Agrawal GP. Nonlinear fiber optics. Berlin, Heidelberg: Springer; 2013.
25. Dudley JM, Genty G, Coen S. Supercontinuum generation in photonic crystal fiber. Rev Mod Phys. 2006;78:1135–84.
26. New G. Introduction to nonlinear optics. New York: Cambridge University Press; 2011.
27. Ranka JK, Windeler RS, Stentz AJ. Optical properties of high-delta air-silica microstructure optical fibers. Opt Lett. 2000;25:796–8.
28. Cheng TL, Nagasaka K, Tuan TH, Xue XJ, Matsumoto M, Tezuka H, et al. Mid-infrared supercontinuum generation spanning 2.0 to 15.1 μm in a chalcogenide step-index fiber. Opt Lett. 2016;41:2117–20.
29. Belli F, Abdolvand A, Chang W, Travers JC, Russell PS. Vacuum-ultraviolet to infrared supercontinuum in hydrogen-filled photonic crystal fiber. Optica. 2015;2:292–300.
30. Fang S, Yamane K, Zhu J, Zhou C, Zhang Z, Yamashita M. Generation of sub-900- μJ supercontinuum with a two-octave bandwidth based on induced phase modulation in argon-filled hollow fiber. IEEE Photonic Tech L. 2011;23:688–90.
31. Russell PS. Photonic-crystal fibres. J Lightwave Technol. 2006;24:4729–49.
32. Lesko DMB, Timmers H, Xing S, Kowligy A, Lind AJ, Diddams SA. A six-octave optical frequency comb from a scalable few-cycle erbium fibre laser. Nat Photonics. 2021;15:281–6.
33. Elu U, Maidment L, Vamos L, Tani F, Novoa D, Frosz MH, et al. Seven-octave high-brightness and carrier-envelope-phase-stable light source. Nat Photonics. 2021;15:277–80.
34. Hooper L, Kalita M, Devine A, Orec-Archer A, Cloweset J. White light 50 W supercontinuum: roadmap to kW truly white lasers. Proc SPIE. 2015;9344:143–8.

Publisher's Note